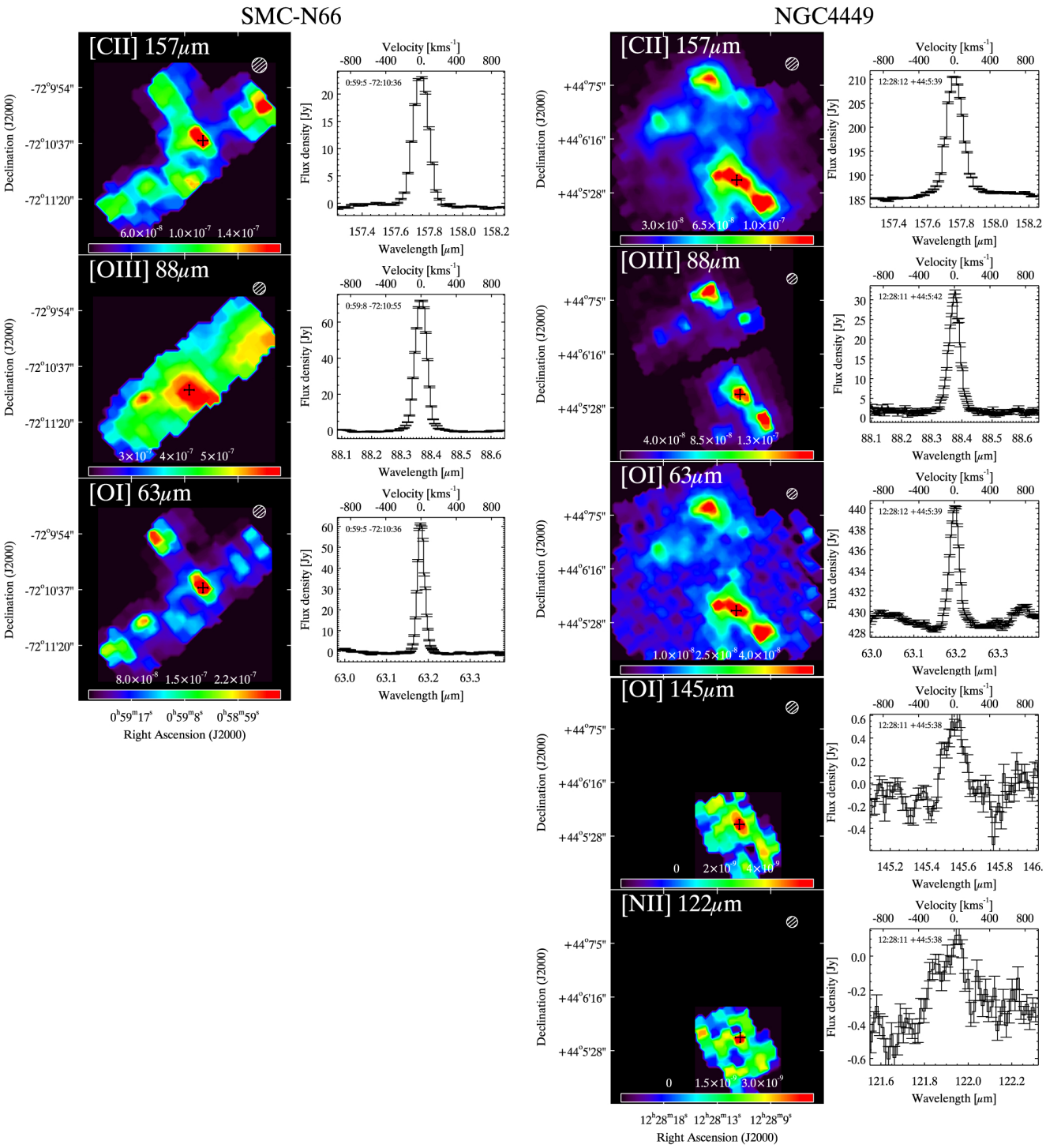

Fig. B.1. continued.

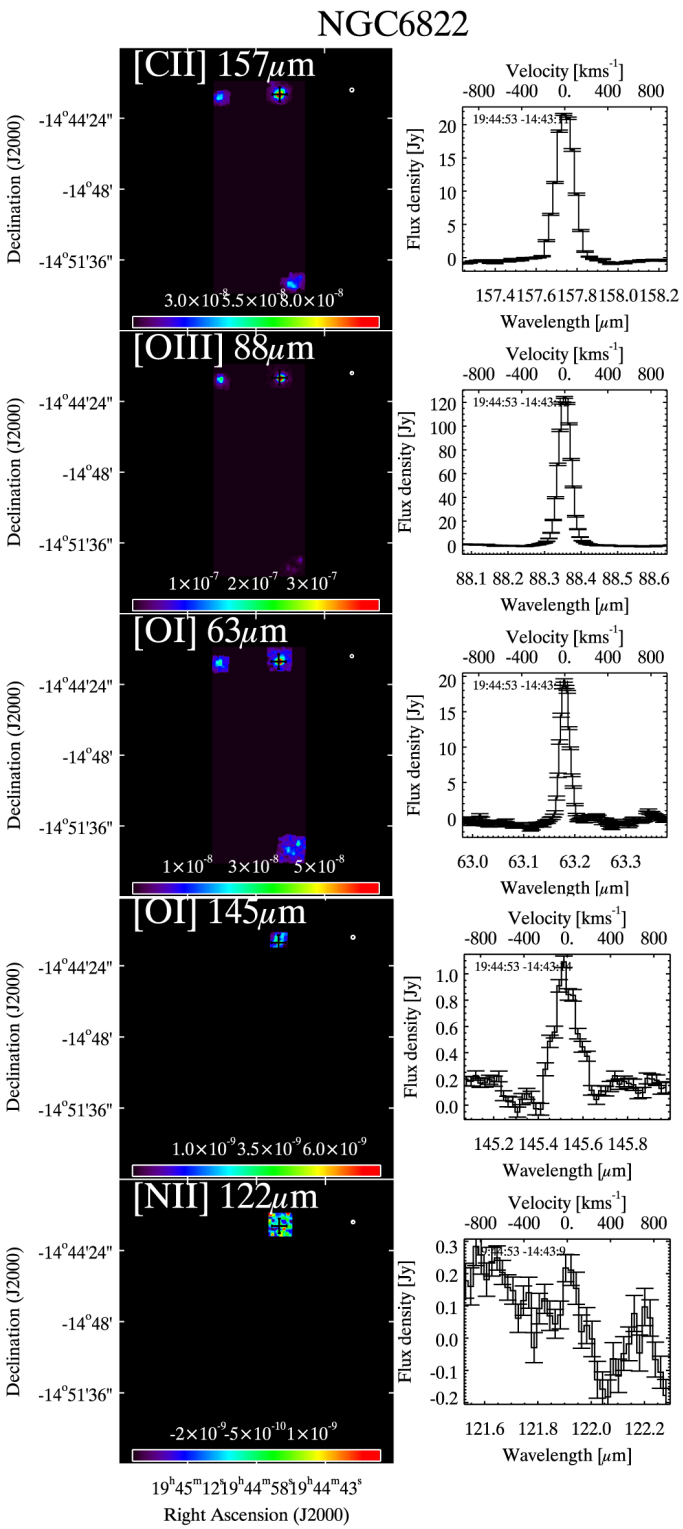

Fig. B.1. continued.

Appendix C: *Spitzer* IRS fluxes of the compact DGS galaxies

We have extracted IRS data of the compact DGS galaxies, as described in Sect. 2.2.1. Fluxes of the main MIR fine-structure cooling lines are listed here (Table C.1 for the low-resolution data and Table C.2 for the high-resolution data).

The spectra of the short and long wavelength modules of the IRS were calibrated using a correction based on the spatial extent of the source. The correction, which is wavelength-dependent, assumes a spherical symmetry for the source shape to account for the light that falls outside the slit. Using this correction, there is no significant flux offsets between the spectra of the short and long wavelength modules for the low-resolution data. For the high-resolution data, extended sources are extracted in different apertures which lead to offsets between the spectra of the short and long wavelength modules. In those cases, the short wavelength spectra are stitched to the long wavelength spectra.

We have compared the overall continuum level of the IRS data to the IRAC and MIPS photometry to verify if all emission is recovered by our reduction (i.e. total flux for the galaxy). This is generally the case, except for NGC 1569 which is clearly more extended than the IRS slit. For reference, we indicate in Table C.1 the ratio of the observed-to-synthetic MIPS 24 μm flux, denoted $R_{\rm MIPS24}$. The observed photometry is from Bendo et al. (2012b) and the synthetic photometry is measured from the IRS data using the MIPS filter profile. This scaling factor should be applied to obtain *total* IRS fluxes. We opt for the 24 μm emission because it arises from active star-forming regions and it is less affected by IRS module stitching than the shorter wavelengths. We note that observed-to-synthetic IRAC 8 μm fluxes are further offset by a factor ~1.8 in 3 galaxies with strong PAH emission (He 2-10, Mrk 1089, NGC 1140). This could be due to PAH (and PDR line) emission outside of the IRS slit as those galaxies show extended structures or to calibration uncertainties.

In Table C.2, we also indicate the average ratio between the high-resolution and low-resolution fluxes of the main spectral lines, denoted HR/LR. Line fluxes generally agree within 20% around that ratio. Differences are mainly due to the extraction method and source extent. [Ne II] and the PAH feature at 12.7 μm, as well as [O IV] and [Fe II] at 25.9 μm, are resolved and thus more accurately measured with the high-resolution mode.

Table C.1. Low-resolution MIR line fluxes in the compact galaxies of the DGS.

Source name	Main observed spectral lines					$R_{\rm MIPS24}$
	[S IV] 10.5 μm	[Ne II] 12.8 μm	[Ne III] 15.6 μm	[S III] 18.7 μm	[S III] 33.5 μm	
Haro 3	3.44 ± 0.16 (×10^2)	3.65 ± 0.12 (×10^2)	–	–	–	–
Haro 11	5.28 ± 0.12 (×10^2)	2.86 ± 0.09 (×10^2)	1.26 ± 0.14 (×10^3)	5.54 ± 0.68 (×10^2)	6.56 ± 0.81 (×10^2)	1.13 ± 0.05
He 2-10	4.25 ± 0.77 (×10^2)	4.17 ± 0.24 (×10^3)	1.50 ± 0.16 (×10^3)	3.24 ± 0.29 (×10^3)	3.79 ± 0.52 (×10^3)	1.13 ± 0.05
HS 0052+2536	13.50 ± 3.07	8.55 ± 1.32	14.97 ± 4.51	21.06 ± 6.28	17.27 ± 4.13	1.15 ± 0.09
HS 0822+3542	5.23 ± 0.47	≤0.50	4.35 ± 1.54	≤1.84	≤2.33	0.88 ± 0.10
HS 1222+3741	7.80 ± 1.27	≤1.81	≤7.89	≤6.79	≤26.26	–
HS 1304+3529	11.10 ± 1.58	≤1.63	16.24 ± 4.76	16.34 ± 4.99	≤25.44	1.07 ± 0.10
HS 1319+3224	≤6.94	≤1.09	≤3.76	≤7.97	≤11.17	–
HS 1330+3651	8.49 ± 1.10	≤0.85	16.45 ± 6.49	≤17.24	≤16.75	–
HS 1442+4250	6.92 ± 1.58	≤1.12	–	–	–	–
II Zw 40	1.80 ± 0.03 (×10^3)	83.49 ± 5.83	1.48 ± 0.04 (×10^3)	5.79 ± 0.44 (×10^2)	7.81 ± 0.63 (×10^2)	1.18 ± 0.05
I Zw 18	4.34 ± 0.38	≤0.50	7.42 ± 1.40	4.44 ± 1.19	3.36 ± 1.66	1.22 ± 0.08
Mrk 153	18.91 ± 2.00	5.44 ± 1.33	29.92 ± 2.54	19.15 ± 1.77	24.33 ± 8.66	1.33 ± 0.06
Mrk 209	79.92 ± 4.46	≤8.95	–	–	–	–
Mrk 930	1.29 ± 0.20 (×10^2)	30.19 ± 4.27	2.11 ± 0.18 (×10^2)	76.56 ± 8.33	1.41 ± 0.17 (×10^2)	1.24 ± 0.05
Mrk 1089	1.48 ± 0.10 (×10^2)	1.80 ± 0.08 (×10^2)	4.71 ± 0.29 (×10^2)	3.05 ± 0.18 (×10^2)	5.27 ± 0.83 (×10^2)	1.27 ± 0.06
Mrk 1450	69.77 ± 3.19	10.69 ± 1.86	94.68 ± 3.29	49.60 ± 4.48	62.92 ± 6.03	1.07 ± 0.05
NGC 1140	1.81 ± 0.10 (×10^2)	1.59 ± 0.07 (×10^2)	4.78 ± 0.20 (×10^2)	2.47 ± 0.19 (×10^2)	4.36 ± 0.96 (×10^2)	1.26 ± 0.05
NGC 1569	–	–	2.73 ± 0.16 (×10^3)	1.38 ± 0.07 (×10^3)	2.50 ± 0.37 (×10^3)	3.16 ± 0.14
Pox 186	36.29 ± 3.66	0.95 ± 0.25	13.81 ± 3.33	7.37 ± 1.25	≤4.64	0.86 ± 0.09
SBS 0335-052	20.04 ± 2.10	1.35 ± 0.56	17.35 ± 2.71	4.24 ± 1.60	≤5.81	1.02 ± 0.05
SBS 1159+545	3.91 ± 1.78	≤2.51	≤3.32	7.06 ± 1.96	≤6.92	1.10 ± 0.13
SBS 1211+540	3.10 ± 0.66	≤1.15	4.94 ± 0.73	3.44 ± 1.32	≤16.72	1.25 ± 0.41
SBS 1249+493	4.74 ± 0.91	≤0.57	9.85 ± 3.89	≤11.72	≤16.27	0.85 ± 0.17
SBS 1415+437	13.95 ± 0.60	3.10 ± 1.23	–	–	–	–
SBS 1533+574	28.93 ± 2.87	4.28 ± 0.51	49.49 ± 9.09	14.10 ± 1.53	25.28 ± 5.94	–

Notes. Fluxes are in 10^{-18} W m^{-2}. Upper limits are given at 2σ.

Table C.1. continued.

Source name	Main observed spectral lines					R_{MIPS24}
	[S IV] 10.5 μm	[Ne II] 12.8 μm	[Ne III] 15.6 μm	[S III] 18.7 μm	[S III] 33.5 μm	
Tol 1214-277	10.53 ± 2.41	≤1.52	5.89 ± 2.48	≤5.10	≤7.11	1.19 ± 0.11
UM 448	2.21 ± 0.11 ($\times10^2$)	3.76 ± 0.22 ($\times10^2$)	6.93 ± 0.83 ($\times10^2$)	3.24 ± 0.19 ($\times10^2$)	6.63 ± 0.48 ($\times10^2$)	1.03 ± 0.04
UM 461	45.89 ± 4.23	2.53 ± 0.62	25.61 ± 6.50	11.91 ± 1.88	11.96 ± 3.76	1.03 ± 0.10

Source name	Other observed spectral lines				
	[Ar II] 6.99 μm	[Ne V] 14.3 μm	[O IV] 25.9 μm	[Si II] 34.8 μm	[Ne III] 36.0 μm
Haro 3	≤56.13	–	–	–	–
Haro 11	37.83 ± 11.61	≤91.56	≤35.97	5.16 ± 1.31 ($\times10^2$)	≤3.75 ($\times10^2$)
He 2-10	4.94 ± 0.43 ($\times10^2$)	1.72 ± 0.73 ($\times10^2$)	≤9.42 ($\times10^2$)	2.41 ± 0.42 ($\times10^3$)	≤1.24 ($\times10^3$)
HS 0052+2536	≤4.04	≤7.35	≤3.11	25.71 ± 7.21	–
HS 0822+3542	≤2.44	≤2.14	≤0.85	2.45 ± 0.92	≤6.18
HS 1222+3741	≤3.04	≤3.99	≤7.75	≤53.57	–
HS 1304+3529	≤8.49	≤6.02	≤6.11	≤24.22	≤16.16
HS 1319+3224	–	≤5.44	≤1.34	9.70 ± 3.12	≤24.74
HS 1330+3651	≤3.38	≤16.31	≤4.68	≤25.65	≤35.09
HS 1442+4250	≤4.40	–	–	–	–
II Zw 40	≤34.98	≤62.44	96.47 ± 39.45	4.51 ± 0.49 ($\times10^2$)	≤1.99 ($\times10^2$)
I Zw 18	≤1.36	≤5.05	≤2.96	8.10 ± 2.76	≤10.18
Mrk 153	≤14.23	≤5.44	≤4.89	18.98 ± 7.45	≤21.97
Mrk 209	≤26.98	–	–	–	–
Mrk 930	≤28.00	≤9.00	≤10.31	1.08 ± 0.08 ($\times10^2$)	≤68.98
Mrk 1089	24.62 ± 7.03	21.44 ± 7.14	≤13.54	2.64 ± 0.51 ($\times10^2$)	≤1.86 ($\times10^2$)
Mrk 1450	≤10.97	≤14.09	≤8.63	31.85 ± 3.44	≤11.22
NGC 1140	≤21.00	≤12.66	≤13.72	3.28 ± 0.30 ($\times10^2$)	≤75.12
NGC 1569	–	29.45 ± 8.33	≤6.17 ($\times10^2$)	1.61 ± 0.22 ($\times10^3$)	≤4.83 ($\times10^2$)
Pox 186	≤1.51	≤2.36	≤0.36	≤4.57	≤7.85
SBS 0335-052	≤2.22	≤6.33	≤5.01	5.61 ± 1.89	≤11.93
SBS 1159+545	≤11.99	≤5.40	≤0.95	≤7.34	≤7.62
SBS 1211+540	≤3.13	≤2.75	≤2.01	≤10.29	≤35.40
SBS 1249+493	≤9.53	≤20.34	≤4.54	≤45.09	≤27.83
SBS 1415+437	≤4.67	–	–	–	–
SBS 1533+574	≤2.66	≤7.76	≤9.59	20.62 ± 2.84	≤11.13
Tol 1214-277	≤16.92	≤4.59	≤5.61	≤7.28	13.18 ± 3.27
UM 448	55.15 ± 25.71	≤38.84	≤10.29	4.89 ± 0.49 ($\times10^2$)	≤1.28 ($\times10^2$)
UM 461	≤4.73	≤8.43	≤3.83	11.87 ± 2.84	≤16.98

Table C.2. High-resolution MIR line fluxes in the compact galaxies of the DGS.

Source name	Main observed spectral lines					*HR*/*LR*
	[S IV] 10.5 μm	[Ne II] 12.8 μm	[Ne III] 15.6 μm	[S III] 18.7 μm	[S III] 33.5 μm	
Haro 3	4.08 ± 0.17 ($\times10^2$)	3.52 ± 0.13 ($\times10^2$)	9.84 ± 0.74 ($\times10^2$)	5.03 ± 0.39 ($\times10^2$)	8.51 ± 0.24 ($\times10^2$)	1.08
Haro 11*	4.94 ± 0.11 ($\times10^2$)	3.27 ± 0.09 ($\times10^2$)	1.12 ± 0.05 ($\times10^3$)	5.31 ± 0.29 ($\times10^2$)	8.17 ± 0.70 ($\times10^2$)	1.04
He 2-10	3.27 ± 0.13 ($\times10^2$)	3.80 ± 0.13 ($\times10^3$)	1.56 ± 0.05 ($\times10^3$)	2.67 ± 0.19 ($\times10^3$)	3.17 ± 0.10 ($\times10^3$)	0.88
HS 0822+3542*	6.43 ± 0.45	≤0.24	2.63 ± 0.21	1.32 ± 0.22	–	0.92
HS 1442+4250*	8.21 ± 0.30	≤0.51	3.83 ± 0.68	1.69 ± 0.59	3.10 ± 1.03	1.19
II Zw 40	2.00 ± 0.10 ($\times10^3$)	73.52 ± 7.93	1.41 ± 0.09 ($\times10^3$)	5.21 ± 0.22 ($\times10^2$)	7.82 ± 0.21 ($\times10^2$)	0.97
I Zw 18	5.69 ± 1.42	≤2.91	7.89 ± 1.02	5.04 ± 1.29	3.94 ± 0.91	1.17
Mrk 153	24.01 ± 5.47	3.91 ± 0.77	31.22 ± 1.72	14.19 ± 2.32	28.89 ± 6.97	0.99
Mrk 209*	85.71 ± 2.88	2.45 ± 0.31	54.49 ± 1.74	24.34 ± 1.49	49.69 ± 5.70	1.07
Mrk 930	1.39 ± 0.05 ($\times10^2$)	39.39 ± 2.44	2.12 ± 0.06 ($\times10^2$)	94.43 ± 4.98	1.28 ± 0.11 ($\times10^2$)	1.12
Mrk 1450*	72.84 ± 1.22	9.18 ± 0.72	93.06 ± 3.32	43.88 ± 1.54	70.17 ± 17.05	0.98
NGC 1140	1.80 ± 0.10 ($\times10^2$)	1.83 ± 0.09 ($\times10^2$)	6.28 ± 0.40 ($\times10^2$)	3.31 ± 0.17 ($\times10^2$)	4.34 ± 0.14 ($\times10^2$)	1.16
NGC 1569	2.47 ± 0.03 ($\times10^3$)	3.05 ± 0.27 ($\times10^2$)	3.24 ± 0.13 ($\times10^3$)	1.31 ± 0.05 ($\times10^3$)	1.85 ± 0.06 ($\times10^3$)	0.96
SBS 0335-052*	14.75 ± 0.37	0.72 ± 0.09	12.37 ± 0.74	3.49 ± 1.05	4.70 ± 1.58	0.71
SBS 1159+545*	≤5.10	≤2.19	≤2.97	≤4.23	≤12.83	n.a.
SBS 1415+437*	12.02 ± 0.92	2.31 ± 0.29	11.33 ± 0.99	7.58 ± 1.20	14.04 ± 3.42	0.81
Tol 1214-277	8.86 ± 0.47	≤1.56	5.57 ± 0.55	≤2.99	≤11.06	0.89
UM 448	2.32 ± 0.04 ($\times10^2$)	3.14 ± 0.12 ($\times10^2$)	6.38 ± 0.25 ($\times10^2$)	3.21 ± 0.12 ($\times10^2$)	4.92 ± 0.21 ($\times10^2$)	0.92
UM 461*	46.71 ± 0.90	1.58 ± 0.39	29.11 ± 1.24	8.71 ± 0.80	12.64 ± 4.60	0.86
NGC 625	5.72 ± 0.07 ($\times10^2$)	1.66 ± 0.05 ($\times10^2$)	7.46 ± 0.26 ($\times10^2$)	4.40 ± 0.15 ($\times10^2$)	7.78 ± 0.39 ($\times10^2$)	n.a.
UM 311	36.80 ± 2.91	43.77 ± 13.69	1.03 ± 0.05 ($\times10^2$)	76.28 ± 5.09	59.99 ± 14.60	n.a.
VII Zw 403	14.47 ± 1.42	5.09 ± 0.34	23.05 ± 2.60	18.49 ± 2.88	≤13.60	n.a.

Source name	Other observed spectral lines				
	[Ar II] 6.99 μm	[Ne V] 14.3 μm	[O IV] 25.9 μm	[Si II] 34.8 μm	[Ne III] 36.0 μm
Haro 3	–	≤14.50	17.93 ± 5.00	3.99 ± 0.24 ($\times10^2$)	1.17 ± 0.29 ($\times10^2$)
Haro 11*	–	≤5.29	43.90 ± 7.84	5.58 ± 0.45 ($\times10^2$)	≤1.92 ($\times10^2$)
He 2-10	–	≤20.84	79.15 ± 25.14	1.93 ± 0.04 ($\times10^3$)	≤2.92 ($\times10^2$)
HS 0822+3542*	–	≤1.02	–	–	–
HS 1442+4250*	–	≤0.43	2.37 ± 0.74	3.40 ± 1.39	≤7.32
II Zw 40	–	≤7.46	79.36 ± 11.53	3.68 ± 0.35 ($\times10^2$)	1.74 ± 0.39 ($\times10^2$)
I Zw 18	–	≤4.02	≤4.08	≤4.37	≤10.87
Mrk 153	–	≤3.45	5.10 ± 1.92	23.78 ± 6.17	≤15.73
Mrk 209*	–	≤1.87	13.13 ± 2.81	32.37 ± 4.07	16.53 ± 7.43
Mrk 930	–	≤3.29	12.02 ± 2.65	1.27 ± 0.12 ($\times10^2$)	34.56 ± 13.98
Mrk 1450*	–	≤1.04	8.31 ± 0.88	30.72 ± 5.42	≤15.28
NGC 1140	–	≤9.94	19.84 ± 3.91	2.71 ± 0.15 ($\times10^2$)	33.81 ± 16.15
NGC 1569	–	≤8.18	3.19 ± 0.15 ($\times10^2$)	1.15 ± 0.03 ($\times10^3$)	≤5.77 ($\times10^2$)
SBS 0335-052*	–	≤1.63	5.22 ± 1.15	≤10.55	≤17.39
SBS 1159+545*	–	≤3.64	≤2.35	≤13.85	≤18.92
SBS 1415+437*	–	≤1.17	6.51 ± 2.02	17.77 ± 3.91	≤7.60
Tol 1214-277*	–	≤0.75	5.43 ± 2.08	≤8.89	–
UM 448	–	≤5.64	30.85 ± 6.35	4.92 ± 0.21 ($\times10^2$)	≤77.59
UM 461*	–	≤0.72	2.77 ± 0.90	8.76 ± 2.71	≤20.95
NGC 625	–	≤31.40	≤3.89	1.85 ± 0.12 ($\times10^2$)	68.04 ± 22.33
UM 311	–	≤2.55	6.39 ± 2.62	56.23 ± 5.82	≤17.00
VII Zw 403	–	≤5.13	≤1.78	≤12.35	≤16.00

Notes. Fluxes are in 10^{-18} W m^{-2}. Upper limits are given at 2σ. The symbol $^{(*)}$ indicates point-like sources reduced with the optimal extraction method. The other sources are extracted from the full apertures. We note that the observation of Pox 186 (AOR key 9007360) is not included because it is not centered on the source.

Appendix D: IRAS and PACS photometry of the compact sample

Table D.1. $L_{\rm TIR}$, IRAS 60/100, and PACS 70/100 band ratios.

Source name	60/100	70/100	$L_{\rm TIR}$
Compact sample			
Haro 11	1.21	1.26	1.98×10^{11}
Haro 2	0.88	0.93	6.38×10^{9}
Haro 3	0.73	0.92	5.43×10^{9}
He 2-10	0.89	1.02	5.49×10^{9}
HS 0017+1055	[1.15]	1.40	9.70×10^{8}
HS 0052+2536	[0.72]	1.06	1.62×10^{10}
HS 0822+3542	[0.67]	1.11	1.05×10^{7}
HS 1222+3741	[0.88]	0.69	2.40×10^{9}
HS 1236+3937	–	0.83	–
HS 1304+3529	[0.80]	0.80	1.69×10^{9}
HS 1319+3224	[0.82]	0.98	2.37×10^{8}
HS 1330+3651	[0.63]	0.83	1.37×10^{9}
HS 1442+4250	–	1.68	–
HS 2352+2733	–	2.52	–
II Zw 40	0.99	1.11	2.89×10^{9}
I Zw 18	[1.74]	2.46	3.34×10^{7}
Mrk 1089	0.67	0.94	3.68×10^{10}
Mrk 1450	0.49	1.22	3.03×10^{8}
Mrk 153	0.59	0.93	1.05×10^{9}
Mrk 209	0.97	0.95	2.98×10^{7}
Mrk 930	0.59	0.81	1.95×10^{10}
NGC 1140	0.68	0.95	3.73×10^{9}
NGC 1569	0.93	1.05	1.27×10^{9}
NGC 1705	0.48	0.80	6.29×10^{7}
NGC 2366	0.75	0.83	1.54×10^{8}
NGC 4214	0.62	0.76	5.34×10^{8}
NGC 4861	0.76	1.02	3.51×10^{8}
NGC 5253	1.00	1.01	1.63×10^{9}
NGC 625	0.66	0.61	2.85×10^{8}
Pox 186	[0.73]	0.74	5.64×10^{7}
SBS 0335-052	[2.76]	2.30	1.76×10^{9}
SBS 1159+545	[1.03]	1.01	2.00×10^{8}
SBS 1211+540	[1.28]	1.91	2.86×10^{7}
SBS 1249+493	[0.75]	0.93	9.34×10^{8}
SBS 1415+437	[1.00]	1.15	6.54×10^{7}
SBS 1533+574	0.63	0.75	2.04×10^{9}
Tol 1214-277	[0.83]	0.96	8.84×10^{8}
UGC 4483	[0.96]	0.43	2.60×10^{6}
UM 133	[0.73]	0.97	1.13×10^{8}
UM 311	[0.44]	0.57	5.61×10^{9}
UM 448	0.93	n.a.	9.00×10^{10}
UM 461	[0.93]	1.48	7.24×10^{7}
VII Zw 403	0.43	0.84	1.99×10^{7}
Extended sample			
IC 10	[0.93]	0.68	7.30×10^{-5}
LMC-30Dor	[1.47]	n.a.	1.11×10^{-3}
LMC-N11A	[0.90]	n.a.	7.92×10^{-5}
LMC-N11B	[1.16]	n.a.	1.67×10^{-4}
LMC-N11C	[1.09]	n.a.	8.99×10^{-5}
LMC-N11I	[0.90]	n.a.	3.01×10^{-5}
LMC-N158	[1.08]	n.a.	2.41×10^{-4}
LMC-N159	[1.18]	n.a.	4.79×10^{-4}
LMC-N160	[1.34]	n.a.	9.34×10^{-4}
NGC 4449	[1.06]	0.65	2.65×10^{-5}
NGC 6822	[0.87]	0.86	2.78×10^{-5}
SMC-N66	[1.15]	n.a.	4.13×10^{-5}

Notes. n.a.: not observed in the PACS 70 μm or 100 μm band. $L_{\rm TIR}$ are SED-integrated values between 3–1100 μm, in units of solar luminosity for the compact sample and W m^{-2} sr^{-1} (peak surface brightness) for the extended sample. The synthetic IRAS fluxes, indicated in brackets, are derived from the SED modeling of Rémy-Ruyer et al. (in prep.).

Appendix E: Line broadening and rotation in the PACS maps

We find that the [O III]$_{88}$ and [O I]$_{63}$ lines, which are bright with smallest instrumental FWHM, are the most often broadened. The line widths are typically ~100 km s^{-1} larger than the instrumental profile in the brightest sources. For the fainter lines, it is more difficult to determine confidently whether or not broadening is present. Broadening of the [C II]$_{157}$ line can only be accurately calculated for intrinsic line widths larger than 150 km s^{-1} because of its large instrumental FWHM of 240 km s^{-1}. When observed, [N III]$_{57}$ is similarly broadened as are [O III]$_{88}$ and [O I]$_{63}$. Such broadening indicates the possible presence of strong turbulent motions, or that multiple components contribute to the emission of those lines. The fact that we find similar intrinsic line widths for all tracers, despite their different origins, indicates that either they are spatially mixed within our beam (which is certainly the case for our compact sources), or that they are affected similarly by the source of this broadening (internal kinematics). Several galaxies also display clear signs of rotation in all observed spectral lines.

Table E.1. Broadening of the FIR lines (in km s^{-1}).

	Broadening						Rotation	
	[N III] $_{57}$	[O I] $_{63}$	[O III] $_{88}$	[N II] $_{122}$	[O I] $_{145}$	[C II] $_{157}$	Axis	$V_{\rm rotation}$
PACS FWHM	105	85	125	290	260	240		
Haro 2	n.a.	90	140	n.a.	n.a.	–	–	–
Haro 3	100	90	110	–	–	–	NEE–SWW	±30 km s^{-1}
Haro 11	160	130	200	200	100	160	N–S	±50 km s^{-1}
He 2-10	160	100	170	–	–	–	NE–SW	±20 km s^{-1}
HS 1330+3651	n.a.	–	150	n.a.	n.a.	–	–	–
II Zw 40	n.a.	80	110	–	–	–	N–S	±30 km s^{-1}
Mrk 1089	n.a.	80	130	–	–	–	NNE–SSW	±80 km s^{-1}
Mrk 153	n.a.	80	120	n.a.	n.a.	–	NE–SW	±30 km s^{-1}
Mrk 930	n.a.	120	120	–	–	–	N–S	±30 km s^{-1}
NGC 1140	n.a.	100	100	–	–	–	NE–SW	±40 km s^{-1}
NGC 1569	n.a.	80	100	n.a.	n.a.	–	–	–
NGC 1705	n.a.	–	100	n.a.	n.a.	–	–	–
NGC 2366	n.a.	80	70	n.a.	n.a.	–	–	-
NGC 4214	n.a.	80	80	–	–	–	–	-
SBS 1533+574	n.a.	–	80	n.a.	n.a.	–	–	–
UM 448	n.a.	150	150	–	80	150	NNE–SSW	±60 km s^{-1}
IC 10	n.a.	90	70	–	–	–	–	-
LMC	150	150	150	100	100	–	–	–
SMC	n.a.	150	150	n.a.	n.a.	–	–	–
NGC 4449	n.a.	90	90	–	–	–	–	–
NGC 5253	n.a.	60	90	–	–	–	NE–SW	±30 km s^{-1}
NGC 6822	n.a.	100	80	–	–	–	–	–

Notes. The broadening (or intrinsic line width) is given as the observed FWHM subtracted by the instrumental FWHM. Uncertainties are on the order of 20%. We indicate the broadening of the spaxel where the emission peaks. This value can be higher elsewhere because of rotation or instrumental effects (uncentered point-source).